SCIENCE CHINA
Chemistry

• ARTICLES •

April 2015 Vol.58 No.4: 627–633
doi: 10.1007/s11426-014-5242-4

Green synthesis of MnO_x nanostructures and studies of their supercapacitor performance

Wei Du[1,2], Xiaoqian Xu[1], Di Zhang[1], Qingyi Lu[1*] & Feng Gao[2*]

[1]*State Key Laboratory of Coordination Chemistry; Nanjing National Laboratory of Microstructures; Coordination Chemistry Institute, School of Chemistry and Chemical Engineering, Nanjing University, Nanjing 210093, China*
[2]*Department of Materials Science and Engineering, Nanjing University, Nanjing 210093, China*

Received June 18, 2014; accepted July 7, 2014; published online January 6, 2015

Manganese oxides with different crystalline phases and morphologies were prepared by calcining $MnCO_3$ precursors. The $MnCO_3$ precursors with different morphologies were obtained through a green route under hydrothermal conditions with orange pericarp extracting solution as the reducing agent. By calcining the precursor under different temperatures and atmospheres, MnO_x with different stoichiometric ratios (i.e., MnO, MnO_2, Mn_2O_3, and Mn_3O_4) can be obtained. Electrochemical studies reveal that among these manganese oxides, MnO or MnO_2 are more suitable as supercapacitor working electrodes than Mn_2O_3 or Mn_3O_4. They exhibit high specific capacitance up to 296.6 F/g and also possess good cycling stability, which make them potential electrode materials for supercapacitors.

MnO_x nanostructures, green synthesis, supercapacitor

1 Introduction

With the development of the automobile industry, electronic technology and sustainable energy sources, the electrification of transportation and large-scale deployment of renewable energy have become major topics. Finding satisfactory electrical energy storage systems has become one of the most difficult challenges [1,2]. Supercapacitors, because of their fast charging/discharging rate, sustainable cycling life, excellent cycle stability, higher power density than batteries, and higher energy density than conventional dielectric capacitors, have attracted intense interest recently and are poised to become the most important next generation energy storage device [3–6]. As important components of capacitors, electrode materials strongly affect capacitor performance. Previously, the widely used electrode materials for supercapacitors are carboneous materials, hybrid composites, conducting polymers, and transition-metal oxides [7–9]. Transition-metal oxides such as manganese oxides (MnO_x) have been researched as electrode materials due to their low cost, environmentally friendliness and superior capacitor performance. However, limited electric conductivity and small accessible surface areas are two key weaknesses of metal oxide materials [10,11]. Two main ways have been adopted to solve these problems. Binary composites (e.g., MnO_x-carbon nanotube [12,13], MnO_x-graphene sheets [14–16], MnO_x-conductive polymers [17–19], vanadium metal and cobalt oxide doped MnO_x [20,21]) and ternary composites (Au-MnO_2/carbon nanotube [22], MnO_2 nanospheres/carbon nanotubes/conducting polymer [23], Zn_2SnO_4/MnO_2 core/shell nanocable-carbon microfiber [24]) of hydrous MnO_x have been explored to effectively utilize and perfect the electrochemical performance of MnO_x materials. However, electrodes made of hydrous MnO_2 with conducting polymers have shown mechanical instability and poor cyclability [10]. For the composites with carbonaceous materials, enhancement of electrochemical performance can be accomplished only when small amounts of metal oxide

*Corresponding authors (email: qylu@nju.edu.cn; fgao@nju.edu.cn)

are incorporated in the electrode [25]. The design and fabrication of ternary composites are also limited due to the complexity of their synthesis and other unique restrictions. For practical applications, particularly large-capacitor applications such as power sources for a hybrid electric vehicle (HEV) or fuel-cell electric vehicle (FCEV), high metal-oxide concentration in electrodes and high mass-loading of total active materials are needed. On the other hand, MnO_x materials with nanostructures can provide a relatively short diffusion path and high surface area to improve the utilization of supercapacitor electrodes [23]. Hierarchical nanostructures and ultrafine nanostructures with diameters of less than 10 nm have therefore attracted great interest due to their higher surface areas, which are especially desirable for supercapacitors [26–28]. Many different methods including electrochemical route, sol-gel method, and hydrothermal and solvothermal techniques, have been developed for the synthesis of MnO_x nanostructures [29–31]. We employed a green chemical route to fabricate a series of manganese oxide nanostructures. By simply refluxing orange pericarp in distilled water, an extracting solution was generated, which we then used as reducing agent to react with commercial $KMnO_4$; fusiform or cubic $MnCO_3$ precursors can be obtained through simple hydrothermal technique. By calcining the precursor at different temperatures and in different atmospheres, fusiform or cubic MnO_x nanostructures with different stoichiometric ratios (e.g., MnO, MnO_2, Mn_2O_3, and Mn_3O_4) can be systematically obtained. We also investigated the influence of morphologies and crystalline structures on the electrochemical performances of the obtained MnO_x materials as supercapacitor electrodes and found that MnO and MnO_2 are more suitable as supercapacitor working electrodes than Mn_2O_3 and Mn_3O_4.

2 Experimental

2.1 Synthesis

$MnCO_3$ precursors were synthesized through the reaction between pericarp extracting solution and $KMnO_4$. In a typical procedure, 12 g of orange pericarp and 150 mL of deionized water were added into a 250 mL round-bottom flask and refluxed under magnetic stirring at a temperature of 105 °C for 5 h. After cooling to room temperature, the obtained suspension was centrifuged at 4000 r/min; the upper liquid was the so-called orange pericarp extracting solution. Next, 10 mL of the extracting solution was transferred into a Teflon lined stainless steel autoclave and mixed with a certain amount of $KMnO_4$. After the solution was stirred for 15 min, the autoclave was sealed and heated at 160 °C for 6 h under hydrothermal conditions. The precipitate product at the bottom of the autoclave was collected after being cooled to room temperature and washed with distilled water. By adding different amounts of $KMnO_4$ to 10 mL of orange pericarp extracting solution, $MnCO_3$ precursors with different morphologies were obtained. For the synthesis of MnO_x structures, the as-prepared precursors were heated in air or in N_2 atmosphere to 400, 600 and 800 °C with a ramping rate of 1 °C/min and kept for 1 h.

2.2 Characterizations

Scanning electron microscopy (SEM) images were acquired on a Hitachi S-4800 (Japan) field-emission scanning electron microscope at an acceleration voltage of 10.0 kV. Crystallographic phases of all the products were investigated by powder X-ray diffraction (XRD) on a Switzerland ARL X'TAR with Cu-Kα irradiation (λ=1.5406 Å).

2.3 Electrochemical tests

We systematically investigated the electrochemical performances of all of the obtained manganese oxides (MnO_x, including +2, +3, +4 oxides and mixed-valence-state oxides). The MnO_x electrodes were prepared by mixing MnO_x powder (80 wt%) as the active material with acetylene black (15 wt%) and polytetrafluoroethylene (PTFE, 5 wt%). The mixture was pressed onto a nickel grid that served as a current collector. The typical mass load of such an electrode material is about 3 mg. Electrochemical performance of the MnO_x electrodes was demonstrated on a CHI 660D electrochemical workstation. The standard three-electrode system was composed of Ag/AgCl as the reference electrode, Pt filament as the counter electrode, and the as-prepared MnO_x electrode as the working electrode.

3 Results and discussion

Dark brown precipitates were obtained after the orange pericarp extracting solution reacted with $KMnO_4$ under the previously described hydrothermal conditions. Figure 1(a) shows the XRD pattern of the product prepared with 0.079 g of $KMnO_4$ and 10 mL of the orange pericarp extracting solution. All of the diffraction peaks can be indexed as rhombohedral $MnCO_3$ according to JCPDS card No. 44-1472. The strong, narrow peaks indicate that the asprepared $MnCO_3$ was in good crystallinity. No other diffraction peaks arising from any other impurities could be detected, which further indicated the high purity of the product. Figure 1(b), which shows an SEM image of the obtained $MnCO_3$ crystallites, confirms that the product was composed of a great number of fusiform particles with an average length of 1 μm. From the enlarged SEM image (insert of Figure 1(b)), it can be seen that the fusiform particles are composed of many short nanowires. When different amounts of $KMnO_4$ were used to react with 10 mL of the orange pericarp extraction solution, $MnCO_3$ with different morphology was synthesized. Figure 1(c), which shows the XRD pattern of the product prepared with 0.237 g of

$KMnO_4$ and 10 mL of the orange pericarp extracting solution, also confirms the formation of rhombohedral $MnCO_3$. However, the SEM images shown in Figure 1(d) reveal that the obtained $MnCO_3$ product was composed of many cubic particles. It is known that orange pericarp contains large amounts of carbohydrates and their derivatives that can be extracted into solution after being refluxed at high temperatures. These molecules, which contain a large number of hydroxyl groups, serve as effective reducing agents. Under certain hydrothermal conditions, these molecules reduce $KMnO_4$ to Mn^{2+} and the generated CO_2 can react with Mn^{2+} to form $MnCO_3$ crystallites. These molecules are also a kind of water-soluble biopolymer and can act as a crystal-growth modifier. As the amount of the used $KMnO_4$ amount changes, so does the ratio of the biopolymer to $KMnO_4$ in the system. As a result, the way that biopolymer assembles also changes and different morphologies of $MnCO_3$ are formed.

By calcining the as-prepared fusiform and cubic $MnCO_3$ precursors in different atmospheres and temperatures, MnO_x nanostructures with different morphologies and crystalline structures can be obtained. Figures 2 and 3 present XRD patterns and SEM images of the calcined products prepared by calcining the two $MnCO_3$ precursors in N_2 at 400, 600 and 800 °C. According to the XRD patterns and JCPDS cards, when the fusiform $MnCO_3$ precursor was calcined at 400 °C, it was decomposed and only amorphous manganese oxide was obtained. After increasing the calcining temperature to 600 and to 800 °C, some diffraction peaks appeared that could easily be indexed to crystalline MnO (JCPDS card No. 07-0230). The diffraction peaks became narrower and stronger with the increase of the calcining temperature, which indicated that the crystalline MnO particles grew larger at higher temperatures. When cubic $MnCO_3$ precursor was calcined in N_2, however, crystalline MnO nanoparticles (Figure 2(d, e)) formed when the temperature was 400 or 600 °C. But when the calcined temperature was 800 °C, another manganese oxide Mn_3O_4 formed according to JCPDS card No. 24-0734. From the SEM images shown in Figure 3, it is obvious that the obtained MnO_x samples retained the morphologies of the precursors. But unlike the precursor with a smooth surface, these MnO_x samples had rough and porous surfaces resulting from the decomposition of $MnCO_3$. When the calcining atmosphere was changed to air, the decomposition process of the $MnCO_3$ precursors changed and two other kinds of manganese oxides could be obtained. From the XRD patterns shown in Figure 4, MnO_2 was obtained when the fusiformed $MnCO_3$ precursor was calcined at 400 °C, whereas Mn_2O_3 was obtained when the calcining temperature was 600 or 800 °C. For the cubic $MnCO_3$ precursor, MnO_2 was obtained at 400 or 600 °C, and Mn_2O_3 was obtained at 800 °C. Similar to the results of the products calcined in N_2 atmosphere, the obtained MnO_2 and Mn_2O_3 samples retained the morphologies of their precursors but had rough and porous surfaces resulting from

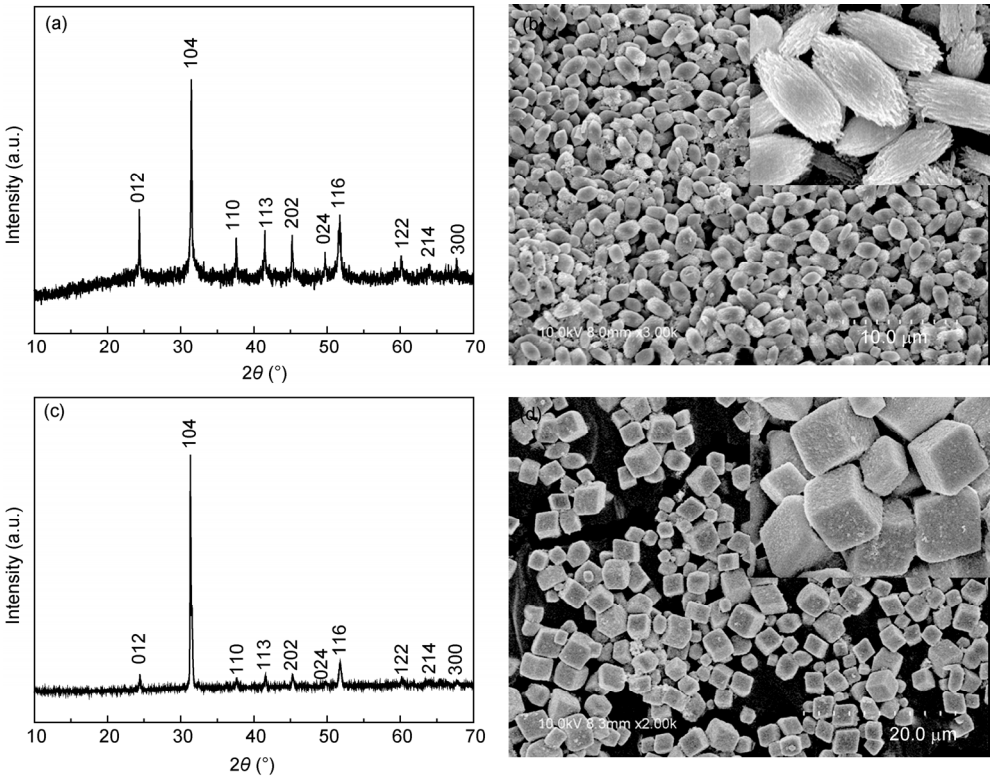

Figure 1 (a) XRD pattern and (b) SEM image of the obtained fusiform $MnCO_3$ precursor; (c) XRD pattern and (d) SEM image of the obtained cubic $MnCO_3$ precursor.

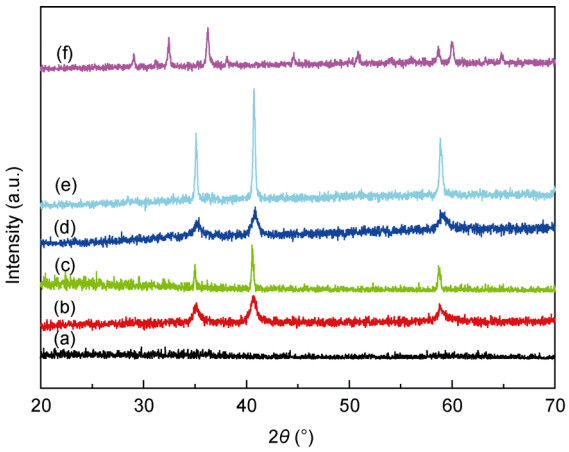

Figure 2 (a–c) XRD patterns of the products prepared by calcining fusiform $MnCO_3$ precursor in N_2 at (a) 400, (b) 600 and (c) 800 °C; (d–f) XRD patterns of the products prepared by calcining cubic $MnCO_3$ precursor in N_2 at (d) 400, (e) 600 and (f) 800 °C.

the decomposition of $MnCO_3$ (Figure 5). The crystalline phases of the obtained manganese oxides are summarized in Table 1. The surface properties of nanomaterials are not only highly dependent upon the crystal shape but also strongly influence nanocrystal activity in chemical reactions [32]. The different morphologies of these two $MnCO_3$ samples would be expected to show different surface activities and lead to different chemical reactions that would generate different valence states of manganese oxides under the same temperatures and atmospheres. These results demonstrate that the green synthesis of MnO_x nanostructures can be realized with orange pericarp. It should be mentioned that other pericarps and naturally occuring plant carbohydrates and their derivatives could also be used to achieve green synthesis.

By calcinating $MnCO_3$ precursors in different atmospheres and at different temperatures, we obtained different manganese oxides with different morphologies that provides great opportunities for us to systematically investigate their properties. We fabricated all of these manganese oxides as supercapacitor working electrodes and evaluated the electrochemical performances by cycle voltammogram (CV) and galvanostatic charge-discharge measurements in 0.5 mol/L Na_2SO_4 solution at room temperature. Figure 6(a, b) shows the typical cycle voltammogram curves of the 12 obtained manganese oxides at a scan rate of 10 mV/s. All of the samples were found to be of highly reversible and ideal capacitive nature with rectangular and symmetrical curves [33,34]. An increasing current magnitude and a more rectangular voltammogram curves indicate better capacitive and higher electrochemical performances [14]. From our investigation of the shape and area of the CV curves in Figure 6(a, b), we found that the obtained MnO or MnO_2 samples would had better electrochemical behaviors than other products (i.e., Mn_3O_4 and Mn_2O_3). We also studied the galvanostatic charge-discharge curves of the MnO_x products (Figure S1, Supporting Information online); Table 2 lists their specific capacitances (SC) calculated from the charge process. Similar to what we observed from the CV curves, MnO and MnO_2 displayed higher specific capacitances than Mn_2O_3 and Mn_3O_4. These results suggest that among these manganese oxides, MnO and MnO_2 are more suitable for supercapacitor working electrodes. In addition, MnO electrodes can acquire higher specific capacitances when the calcining temperatures are lower and the fusiformed and

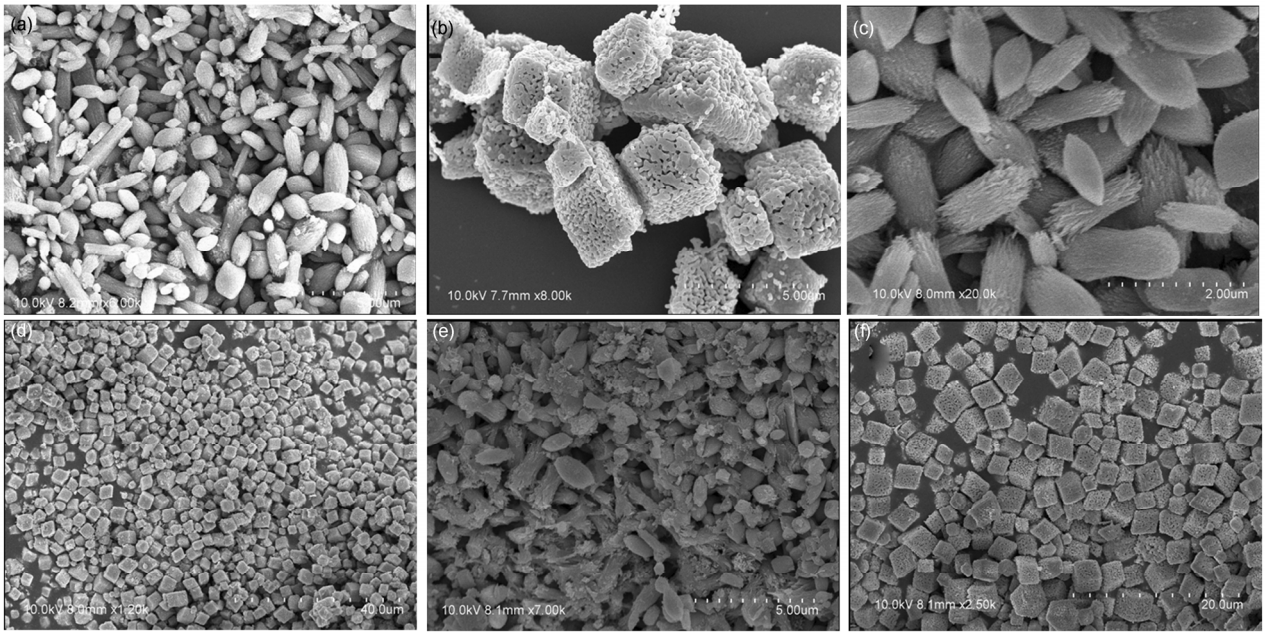

Figure 3 SEM images of the products prepared by calcining fusiform and cubic $MnCO_3$ precursors in N_2 at (a, b) 400, (c, d) 600 and (e, f) 800 °C.

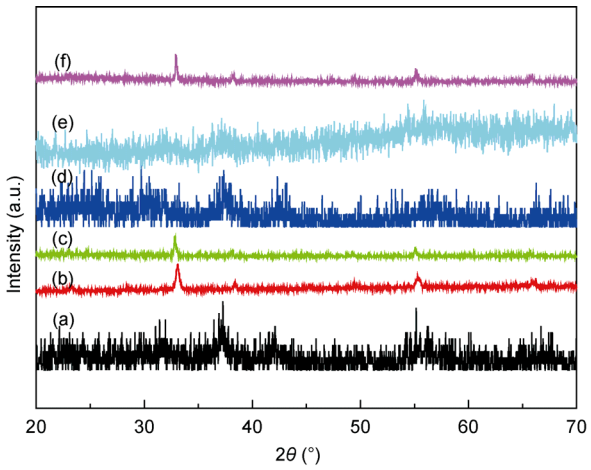

Figure 4 (a–c) XRD patterns of the products prepared by calcining fusiform $MnCO_3$ precursor in the air at (a) 400, (b) 600 and (c) 800 °C; (d–f) XRD patterns of the products prepared by calcining cubic $MnCO_3$ precursor in the air at (d) 400, (e) 600 and (f) 800 °C.

cubic MnO nanostructures obtained at 400 °C show the highest capacitance values (296.2 and 279.1 F/g, respectively). For the obtained MnO_2 samples, the specific capacitance reached 243.1 F/g when the $MnCO_3$ precursor was calcined at 600 °C in air. We tested the BET surface area of the samples (listed in Table 2 with the corresponding specific capacitances). Although the surface area or the morphology might influence the specific capacitance, the data clearly show that the decisive factor for the applicability of electrode materials is the chemical component of the samples. The rate capability is key for the electrode materials of supercapacitors. Figure S2 (Supporting Information online) displays the charge-discharge curves of the four MnO_x materials with good-performances at the current densities of 1, 2, and 5 A/g. At these current densities, the F-N_2-4 (MnO) sample shows better supercapacitor performance than the others. Its specific capacity remains 134.2 F/g when the current density increases to 5 A/g. These results demonstrate that through the green synthesis route and high-temperature calcination, MnO and MnO_2 nanostuctures can be obtained and have potential as working materials for supercapacitors. Because a long cycle-life is very important for supercapacitors, we also ran the cycle charge/discharge tests to examine the service life of the obtained MnO_x nanostructures. Figure 6(c), which displays the specific capacitances of the MnO_x samples with the top four SC values as a function of cycle number at a current density of 2 A/g

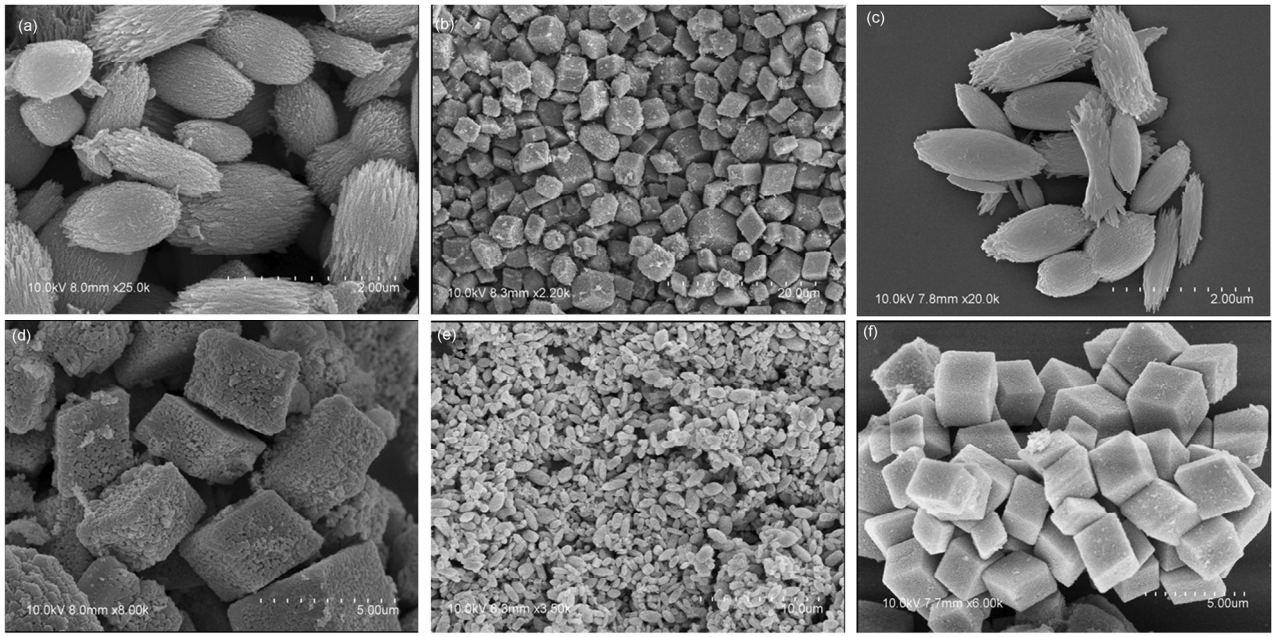

Figure 5 SEM images of the products prepared by calcining fusiform and cubic $MnCO_3$ precursors in the air at (a, b) 400, (c, d) 600 and (e, f) 800 °C.

Table 1 Crystalline phases and denominations of the obtained MnO_x nanostructures by calcining $MnCO_3$ precursors at different temperatures and in different atmosphere

Calcining conditions	In N_2			In the air		
	400 °C	600 °C	800 °C	400 °C	600 °C	800 °C
Fusiforms	F-N_2-4	F-N_2-6	F-N_2-8	F-Air-4	F-Air-6	F-Air-8
	MnO	MnO	MnO	MnO_2	Mn_2O_3	Mn_2O_3
Cubes	C-N_2-4	C-N_2-6	C-N_2-8	C-Air-4	C-Air-6	C-Air-8
	MnO	MnO	Mn_3O_4	MnO_2	MnO_2	Mn_2O_3

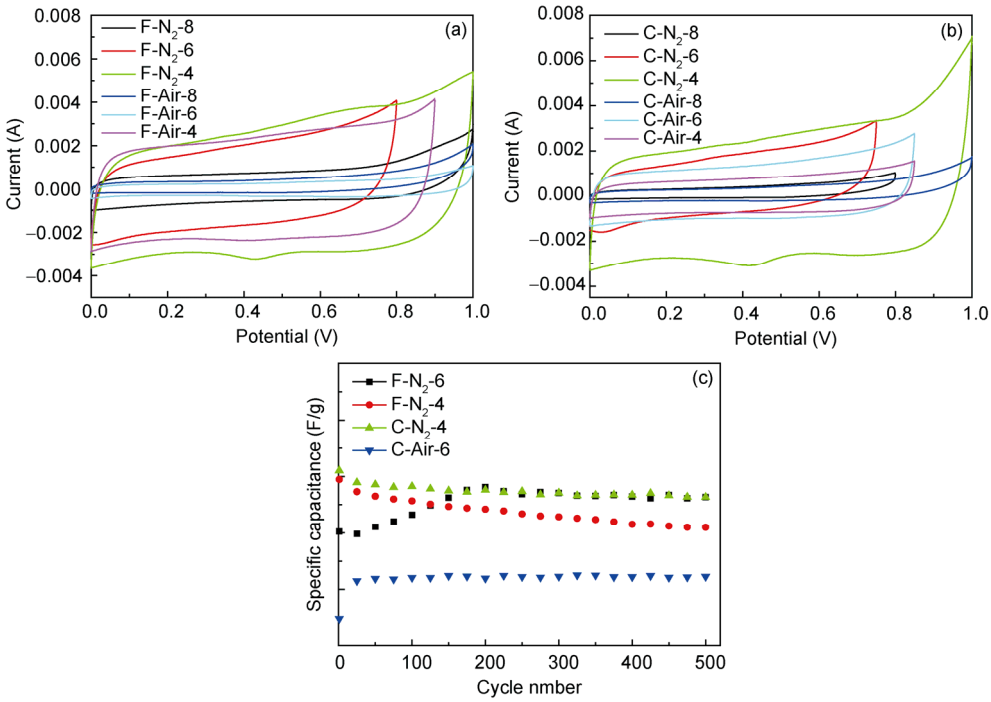

Figure 6 (a) CV curves of the obtained fusiform MnO_x electrode in the potential region of 0.1–0.5 V at a scanning rate of 10 mV/s; (b) CV curves of the obtained cubic MnO_x electrode in the potential region of 0.1–0.5 V at a scanning rate of 10 mV/s; (c) cycling performances of the MnO_x at the current density of 2 A/g.

Table 2 SC with current density of 0.5 A/g and specific surface area (SA) of the obtained MnO_x nanostructures

Calcining conditions		In N_2			In the air		
		400 °C	600 °C	800 °C	400 °C	600 °C	800 °C
Fusiforms		F-N_2-4	F-N_2-6	F-N_2-8	F-Air-4	F-Air-6	F-Air-8
	SC (F/g)	296.2	218.5	49.3	122.5	17.6	23.5
	SA (m^2/g)	106.8	84.9	48.1	102.8	21.2	20.1
Cubes		C-N_2-4	C-N_2-6	C-N_2-8	C-Air-4	C-Air-6	C-Air-8
	SC (F/g)	279.1	93.1	25.9	75.4	243.1	8.6
	SA (m^2/g)	37.5	10.2	2.3	41.2	12.2	4.2

for up to 500 cycles, shows that the obtained MnO or MnO_2 electrodes have very good cycle properties that would make them excellent electrode materials for supercapacitors; in addition, the specific capacitances even grow a little larger after the first 500 cycles (possibly due to an electrochemical activation phenomenon [35]). The electrolyte remains transparent after the cycling test, which indicated minimal dissolution of active materials into solutions and maybe the main cause of the specific capacitance maintenance of manganese oxide-based capacitors [36].

4 Conclusions

Fusiformed and cubic MnO_x nanostructures with different Mn oxidation states were successfully synthesized by a simple hydrothermal route and subsequent calcining process with a green chemistry method by which an extracting solution of orange pericarp was used as both reducing agent and growth modifier. With different dosages of manganese material, fusiform or cubic precursor $MnCO_3$ were obtained. By calcining the obtained $MnCO_3$ precursors at different temperatures and in different calcining atmospheres, different MnO_x nanostructures (e.g., MnO, MnO_2, Mn_2O_3 or Mn_3O_4) were obtained. Electrochemical studies revealed that among these manganese oxides, MnO or MnO_2 were more suitable as supercapacitor working electrodes than Mn_2O_3 or Mn_3O_4. They exhibited high specific capacitance that reach as high as 296.6 F/g and possessed good cycling stability, which make them potential electrode materials for supercapacitors.

Supporting information

The supporting information is available online at chem.scichina.com and link.springer.com/journal/11426. The supporting materials are published as submitted, without typesetting or editing. The responsibility for scientific accuracy and content remains entirely with the authors.

1 Yang ZG, Zhang JL, Kintner-Meyer MCW, Lu XC, Choi D, Lemmon JP, Liu J. Electrochemical energy storage for green grid. *Chem Rev*, 2011, 111: 3577–3613
2 Wagner FT, Lakshmanan B, Mathias MF. Electrochemistry and the future of the automobile. *J Phys Chem Lett*, 2010, 1: 2204–2219
3 Miller JR, Simon P. Electrochemical capacitors for energy management. *Science*, 2008, 321: 651–652
4 Chen LF, Huang ZH, Liang HW, Gao HL, Yu SH. Three-dimensional heteroatom-doped carbon nanofiber networks derived from bacterial cellulose for supercapacitors. *Adv Funct Mater*, 2014, 24: 5104–5111
5 Chen LF, Zhang XD, Liang HW, Kong MG, Guan QF, Chen P, Wu ZY, Yu SH. Synthesis of nitrogen-doped porous carbon nanofibers as an efficient electrode material for supercapacitors. *ACS Nano*, 2012, 6: 7092–7102
6 Chen LF, Huang ZH, Liang HW, Yao WT, Yu ZY, Yu SH. Flexible all-solid-state high-power supercapacitor fabricated with nitrogen-doped carbon nanofiber electrode material derived from bacterial cellulose. *Energy Environ Sci*, 2013, 6: 3331–3338
7 Kaempgen M, Chan CK, Ma J, Cui Y, Gruner G. Printable thin film supercapacitors using single-walled carbon nanotubes. *Nano Lett*, 2009, 9: 1872–1876
8 Zhang LL, Zhou R, Zhao XS. Graphene-based materials as supercapacitor electrodes. *J Mater Chem*, 2010, 20: 5983–5992
9 Wang YG, Li HQ, Xia YY. Ordered whiskerlike polyaniline grown on the surface of mesoporous carbon and its electrochemical capacitance performance. *Adv Mater*, 2006, 18: 2619–2623
10 Sivakkumar SR, Ko JM, Kim DY, Kim BC, Wallace GG. Performance evaluation of CNT/polypyrrole/MnO_2 composite electrodes for electrochemical capacitors. *Electrochim Acta*, 2007, 52: 7377–7385
11 Luo JY, Cheng L, Xia YY. $LiMn_2O_4$ hollow nanosphere electrode material with excellent cycling reversibility and rate capability. *Electrochem Commun*, 2007, 9: 1404–1409
12 Lee SW, Kim J, Chen S, Hammond PT, Yang SH. Carbon nanotube/manganese oxide ultrathin film electrodes for electrochemical capacitors. *ACS Nano*, 2010, 4: 3889–3896
13 Chen PC, Shen GZ, Shi Y, Chen HT, Zhou CW. Preparation and characterization of flexible asymmetric supercapacitors based on transition-metal-oxide nanowire/single-walled carbon nanotube hybrid thin-film electrodes. *ACS Nano*, 2010, 4: 4403–4411
14 Mao L, Zhang K, Chan HSO, Wu JS. Nanostructured MnO_2/graphene composites for supercapacitor electrodes: the effect of morphology, crystallinity and composition. *J Mater Chem*, 2012, 22: 1845–1851
15 Yan J, Fan ZJ, Wei T, Qian WZ, Zhang ML, Wei F. Fast and reversible surface redox reaction of graphene-MnO_2 composites as supercapacitor electrodes. *Carbon*, 2010, 48: 3825–3833
16 Lei ZB, Shi FH, Lu L. Incorporation of MnO_2-coated carbon nanotubes between graphene sheets as supercapacitor electrode. *ACS Appl Mater Interfaces*, 2012, 4: 1058–1064
17 Zhang X, Ji LY, Zhang SC, Yang WS. Synthesis of a novel polyaniline-intercalated layered manganese oxide nanocomposite as electrode material for electrochemical capacitor. *J Power Sources*, 2007, 173: 1017–1023
18 Liu R, Lee SB. MnO_2/poly(3,4-ethylenedioxythiophene) coaxial nanowires by one-step coelectrodeposition for electrochemical energy storage. *J Am Chem Soc*, 2008, 130: 2942–2943
19 Liu R, Duay J, Lee SB. Redox exchange induced MnO_2 nanoparticle enrichment in poly(3,4-ethylenedioxythiophene) nanowires for electrochemical energy storage. A*CS Nano*, 2010, 4: 4299–4307
20 Yang DF. Pulsed laser deposition of cobalt-doped manganese oxide thin films for supercapacitor applications. *J Power Sources*, 2012, 198: 416–422
21 Yang DF. Pulsed laser deposition of vanadium-doped manganese oxide thin films for supercapacitor applications. *J Power Sources*, 2013, 228: 89–96
22 Reddy ALM, Shaijumon MM, Gowda SR, Ajayan PM. Multisegmented Au-MnO_2/carbon nanotube hybrid coaxial arrays for high-power supercapacitor applications. *J Phys Chem C*, 2010, 114: 658–663
23 Hou Y, Cheng YW, Hobson T, Liu J. Design and synthesis of hierarchical MnO_2 nanospheres/carbon nanotubes/conducting polymer ternary composite for high performance electrochemical electrodes. *Nano Lett*, 2010, 10: 2727–2733
24 Bao LH, Zang JF, Li XD. Flexible Zn_2SnO_4/MnO_2 core/shell nanocable-carbon microfiber hybrid composites for high-performance supercapacitor electrodes. *Nano Lett,* 2011, 11: 1215–1220
25 Fischer AE, Pettigrew KA, Rolison DR, Stroud RM, Long JW. Incorporation of homogeneous, nanoscale MnO_2 within ultraporous carbon structures via self-limiting electroless deposition: implications for electrochemical capacitors. *Nano Lett*, 2007, 7: 281–286
26 Jiang J, Li YY, Liu JP, Huang XT, Yuan CZ, Lou XW. Recent advances in metal oxide-based electrode architecture design for electrochemical energy storage. *Adv Mater*, 2012, 24: 5166–5180
27 Fei JB, Cui Y, Yan XH, Qi W, Yang Y, Wang KW, He Q, Li JB. Controlled preparation of MnO_2 hierarchical hollow nanostructures and their application in water treatment. *Adv Mater*, 2008, 20: 452–456
28 Li ZQ, Ding Y, Xiong YJ, Yang Q, Xie Y. One-step solution-based catalytic route to fabricate novel α-MnO_2 hierarchical structures on a large scale. *Chem Commun*, 2005: 918–920
29 Yu P, Zhang X, Wang DL, Wang L, Ma YW. Shape-controlled synthesis of 3D hierarchical MnO_2 nanostructures for electrochemical supercapacitors. *Cryst Growth Des*, 2009, 9: 528–533
30 Duay J, Sherrill SA, Gui Z, Gillette E, Lee SB. Self-limiting electrodeposition of hierarchical MnO_2 and $M(OH)_2$/MnO_2 nanofibril/nanowires: mechanism and supercapacitor properties. *ACS Nano*, 2013, 7: 1200–1214
31 Komaba S, Tsuchikawa T, Ogata A, Yabuuchi N, Nakagawa D, Tomita M. Nano-structured birnessite prepared by electrochemical activation of manganese(III)-based oxides for aqueous supercapacitors. *Electrochim Acta*, 2012, 59: 455–463
32 Tian N, Zhou ZY, Sun SG, Ding Y, Wang ZL. Synthesis of tetrahexahedral platinum nanocrystals with high-index facets and high rlectro-oxidation vctivity. *Science*, 2007, 316: 732–735
33 Yan J, Fan Z, Wei T, Cheng J, Shao B, Wang K, Song L, Zhang M. Carbon nanotube/MnO_2 composites synthesized by microwave-assisted method for supercapacitors with high power and energy densities. *J Power Sources*, 2009, 194: 1202–1207
34 Subramanian V, Zhu HW, Wei BQ. Synthesis and electrochemical characterizations of amorphous manganese oxide and single walled carbon nanotube composites as supercapacitor electrode materials. *Electrochem Commun*, 2006, 8: 827–832
35 Hu CC, Chang KH, Hsu TY. The synergistic influences of OH^- concentration and electrolyte conductivity on the redox behavior of $Ni(OH)_2$/NiOOH. *J Electrochem Soc*, 2008, 155: F196–F200
36 Jiang H, Zhao T, Ma J, Yan CY, Li CZ. Ultrafine manganese dioxide nanowire network for high-performance super capacitors. *Chem Commun*, 2011, 47: 1264–1266